Using wing modal deformation for improvement of CFD results of ESWIRP project

Petr Vrchota
Aerospace Research and Test Establishment (VZLU)
Research Engineer
Beranovych 130, 199 05, Prague, Czech Republic
vrchota@vzlu.cz

Aleš Prachař (Research Scientist, VZLU)

ABSTRACT

A CFD analysis of ESWIRP test campaign at ETW using NASA CRM was done. Two Reynolds number were simulated to evaluate the effect of aeroelasticity on aerodynamic forces and local flowfield. Large difference was noticed between the CFD and experimental data. A model deformation during the wind tunnel tests was the main reason for these differences. A wing modal analysis of CRM was used to include the wing deformation and to improve accuracy of CFD results. On-line mesh deformation using 20 modes in total was used during coupled CFD simulations. It has been shown that the addition of the wing deformation into CFD simulation did improve the accuracy of obtained aerodynamic coefficients, Cp distribution along the wing span and wing deformation. The results from the coupled CFD simulation are the focus of this paper.

1   INTRODUCTION

The flow around an aircraft is usually very complicated and often unsteady due to the vortex-dominated flow. At low-speed condition the vortices are generated by deployed high-lift devices and high α. At high-speed conditions the local flow separation due to shock wave interaction with boundary layer and/or the buffeting may appear. The usability of standard RANS and URANS methods of CFD simulations of these applications could be questionable and therefore it is needed to validate the obtained numerical results by experimental data from the wind tunnels. This study is aimed to evaluate the CFD results of a NASA Common Research Model (CRM) by experimental data. The ESWI[RP] [1] sub-project "Time-resolved wake measurement of separated wing flow and wall interference measurement" is among others focusing on investigation of the effect of the wake emanating from the wing to the Horizontal Tail Plane (HTP) at high-speed condition in presence of buffeting and in the low-speed condition at high angle of attack. The wake from the wing has been visualized by time-resolved PIV method [2], [3]. The results are intended to be used for improvement of the knowledge of the massive flow separation and the effect of the wake on the empennage and also for further verification of the CFD methods. Due to very complex flowfield, loads and deformation of the model the validation of the applied CFD methods is necessary as the first step before analysing the effect of the wake.

The wing tunnel experiments were carried out at ETW [4] and include the aerodynamic force and moment measurement, spanwise pressure distribution at defined locations as well as the wing deformation. A model deformation has indispensable effect on the aerodynamic characteristics in cases that the ratio of dynamic pressure over Young module is high. These cases correspond to the wind tunnel measurements with realistic Reynolds and Mach numbers corresponding to the flight conditions of an airliner [5]. Among other effects the elasticity of a wind tunnel model has to be taken into account during CFD simulations to improve the accuracy [6]. The methods how to implement the model deformation into

CFD simulation ranges from the simple to the complex ones. Among the simplest method belongs the correction of the wing deformation obtained from the comparison of the wind tunnel and CFD results [7]. On the other end there is a coupling between CFD and FEM solvers (Fluid Structure Interaction – FSI) [8]. Between these two methods the usage of the modal analysis, which can be done independently on the CFD simulations and it is not so demanding as FSI, can be found.

2   MODEL

A NASA CRM [9] representing the widebody commercial transport aircraft with a contemporary supercritical transonic wing has been used for this study. The CRM is designed for a cruise Mach number M=0.85 and corresponding design lift coefficient CL=0.5. This model was designed at NASA and among other purposes has been used during the Drag Prediction Workshops (DPW) to obtain the experimental data for CFD code verification. The CRM can be used in various configurations including several settings of Horizontal Tail Plane (HTP), nacelle and pylon. It is equipped with pressure taps to measure the pressure distributions. The wing/body configuration without pylon, nacelle and HTP has been used during this study (see Figure 1). No support system was considered during CFD simulations. Geometry depicted in Figure 1 has been downloaded from CRM website [10].
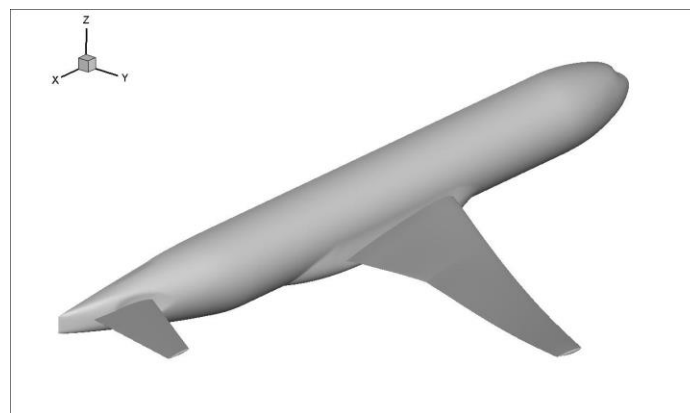
Figure 1 Common Research model

3   METHODS

3.1   Grid generation and flow solver

Two meshes have been used for this study, an in-house and a grid downloaded from the DPW website [11]. The in-house grid has been generated by ICEM-CFD and Tritet solvers [12], [13]. It is an unstructured grid with triangular elements on the model surfaces and with tetrahedra in the volume. The boundary layer is simulated by prismatic elements. The downloaded grid has been provided by DLR and it corresponds to the medium grid from the point of view of number of cells and y+ value. It consists of rectangular elements on the model surfaces, prismatic layer and tetrahedron elements in the volume.
The RANS equations are solved in Edge, FOI's in-house CFD program package [14]. It is a finite volume Navier-Stokes solver for unstructured meshes. The data structure is edge-based, the code is constructed as cell-vertex. It employs local time-stepping, local low-speed preconditioning, multi-grid and dual-time stepping for steady-state and time-dependent problems. The Wallin & Johansson explicit algebraic Reynolds-stress turbulence model [15] was used for this study. All simulations were run as a fully turbulent flow.

The CFD solver has been running in two modes, RANS and URANS, respectively. The solution from the RANS mode served as an initial solution for the URANS simulation. The modal coupling option has been switched on during the URANS simulations and the elasticity of the model has been taken into account.

The upper limit of the polar was limited by value of α=5°. The simulations of this transonic case show buffet on the main wing beginning at α=4.5°. The buffet condition has been also observed at this α during previous experiment [16].

A farfield boundary condition was used on the outer boundary of the computational domain. This condition is specified by Mach number, flow direction, static pressure and static temperature. The aircraft was treated as no-slip viscous wall. Symmetry boundary condition was used at the symmetry plane of the half model.

3.2 Flow conditions

The calculated regimes corresponded to the cases measured during the wind tunnel tests campaign at ETW which has a unique capability to control the pressure, temperature and Mach number independently. It allows separating the Mach, Reynolds numbers and aeroelasticity effects. Freestream Mach number 0.85 and the Re=$5 \cdot 10^6$ and Re=$30 \cdot 10^6$ based on mean aerodynamic chord were calculated. Two Reynolds numbers were chosen to evaluate the effect of dynamic pressure on the model's deformation. Simulations were run over a range of α from 0° to 4°. The static, dynamic and total pressures corresponded to the wind tunnel conditions.

4 MODAL ANALYSIS AND MESH DEFORMATION

4.1 Modal analysis

The modal analysis has been used to obtain the model deformation. The structural model of the whole wind tunnel model airplane has been downloaded from the CRM website [10]. Assuming that the main wing is dominant deforming structure, only half model of the CRM with elastic wing has been considered. To avoid full coupling between the CFD and CSM solver the deformation modelling is based on modal analysis, which was performed in MSC Nastran. The implementation in the Edge solver is described in detail [17], the idea is briefly presented here.

The modal analysis is based on the assumption that the behaviour of the model deformation can be described by the system of equations

$$M\ddot{x} + C\dot{x} + Kx = \text{f}, \tag{1}$$

where x is the vector of structural coordinates, f(t) is the vector of structural forces (aerodynamic forces in our case) and M, C, and K represent the real and symmetric mass, damping and stiffness matrices, respectively. This model can be used for small deformations. The analysis for the special case (C = 0, f = 0) leads to the solution of the generalized eigenvalue problem with a set of eigenvectors ϕ_k (normal modes, representing the displacement) and natural frequencies ω_k. Since the algorithm extracts the eigenvectors in order of increasing ω_k's, it is possible to truncate this expansion after obtaining the first N modes. Twenty modes were used in the present study.

Using the normal modes as a basis set, the time varying coordinates of the (structural) grid can be represented by the sum

$$x(t) = x_0 + \sum_{k=1}^{N} q_k(t)\phi_k, \tag{2}$$

where $q_k(t)$ represents the generalized coordinate of the mode k. Further manipulations and assumptions lead to the system

$$A\ddot{q} + D\dot{q} + Eq = Q,$$ (3)

where A, D and E are diagonal matrices of generalized mass, damping and stiffness, respectively, coupled by the vector of generalized forces Q.

4.2   Mesh deformation

Since the model deformation is obtained on the structural grid it is necessary to interpolate it to the boundary of the CFD grid and to extend the boundary deformation to the volume to obtain a valid CFD grid. A program, which is a part of the Edge package, based on the Moving Least Squares (MLS) method has been used for the first task. The perturbation of any CFD surface node is obtained from the perturbation of the neighbouring structural nodes (number of such nodes is limited by a given radius and/or maximum number of nodes) with linear fit.

The extension of the deformation to the volume is done by the solver during the course of the computation, the Laplacian smoothing algorithm is the basis of the implementation. Although the steady deformation is sought, the solver needs to be run in unsteady mode since the time advancing algorithm is applied to calculate the modal deformation. However, coarse time resolution can be used which makes the efficiency of the process acceptable.

This approach is on one hand less memory consuming and does not require too much work done in the preprocessing phase than the one previously used [18], since the mode shapes are stored only for boundary nodes and not in the whole field, on the other hand the "on-line" mesh deformation is a time consuming procedure which has to be repeated in every time step in the current implementation.

If the solution converges to the steady state, the deformation is in fact proportional to the generalized forces and (inversely proportional) to the entries of the generalized stiffness matrix since the time derivatives of generalized modal coordinates are zero, cf. (3).

5   RESULTS

In the following section the experimental and CFD results are compared. The experimental data were downloaded from the ESWI[RP] project website [1]. The correction on the effect of support system was used on experimental results and therefore the CFD data are directly comparable. The aerodynamic forces, pressure distributions and wing's deformation for particular α's and regimes have been compared. During the comparison of the results, it has been found, that the rigid model over predicted the CL and also CD for both Reynolds numbers. The same trend was observed also during evaluation of the Drag Prediction Workshop [11].

Example of wing deformation for each α corresponds to the contribution of particular modes with regard to their effect. The wing's deformations for particular α corresponding to the Re=$30 \cdot 10^6$ are depicted in Figure 2. The deformation's magnitude has been scaled to emphasize it. The shade one corresponds to the rigid model.
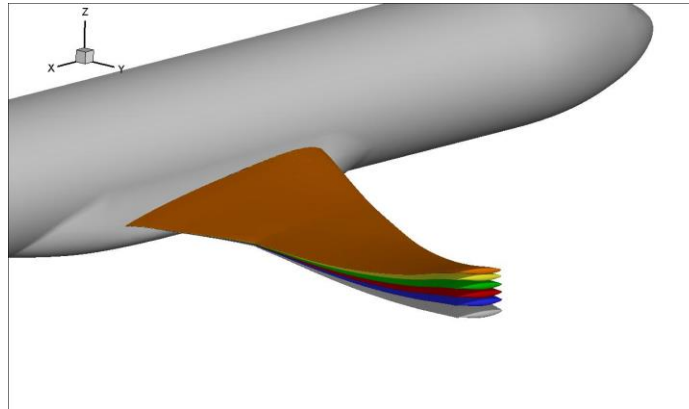
Figure 2 Deformation of the wing for particular AoA

5.1 Aerodynamic forces

Using the elastic model a better match of the CFD and experimental data has been achieved. The elastic model slightly overpredicted CL and underpredicted Cm for both calculated Reynolds numbers. CFD values of CD almost perfectly correspond to the experimental data corrected for the presence of the support system for both regimes in a given range of α. For Re=$5 \cdot 10^6$ the CL is increased by about 3 lift counts at α=0° and by about 0.3 lift counts at α=4°. Similar behaviour was observed for Re=$30 \cdot 10^6$, the CL is increased by about 3 lift counts within the whole range of considered α's. The lift, drag and pitching moment curves of the rigid, elastic model and experiments are depicted in the Figure 3, Figure 4 and Figure 5 corresponding to the Re=$5 \cdot 10^6$ and $30 \cdot 10^6$, respectively. The green lines in the aforementioned Figures corresponded to the corrected experimental values.

Although the experimental data were corrected on the effect of support system, the uncorrected and corrected values of CL and Cm seem to be almost the same. The effect of the support system is visible only on the values of CD. It is in contradiction with [6] and [20] where the effect of support system on CL, CD and Cm was numerically investigated for Re=$5 \cdot 10^6$ and M=0.85. Values of CL and CD were decreased and values of Cm were increased by a small amount. If these corrections of CL and Cm are applied to our CFD results, the same and almost perfect match of lift curve in the linear range of α's is achieved (see Figure 6) and the Cm curves are closer to the experimental values (see Figure 5), although some differences still persist. These differences could be related to the rigid (undeformed) HTP. We believe that similar corrections could be applied to the regime with higher Reynolds number and the results would be also improved from CL and Cm points of view.
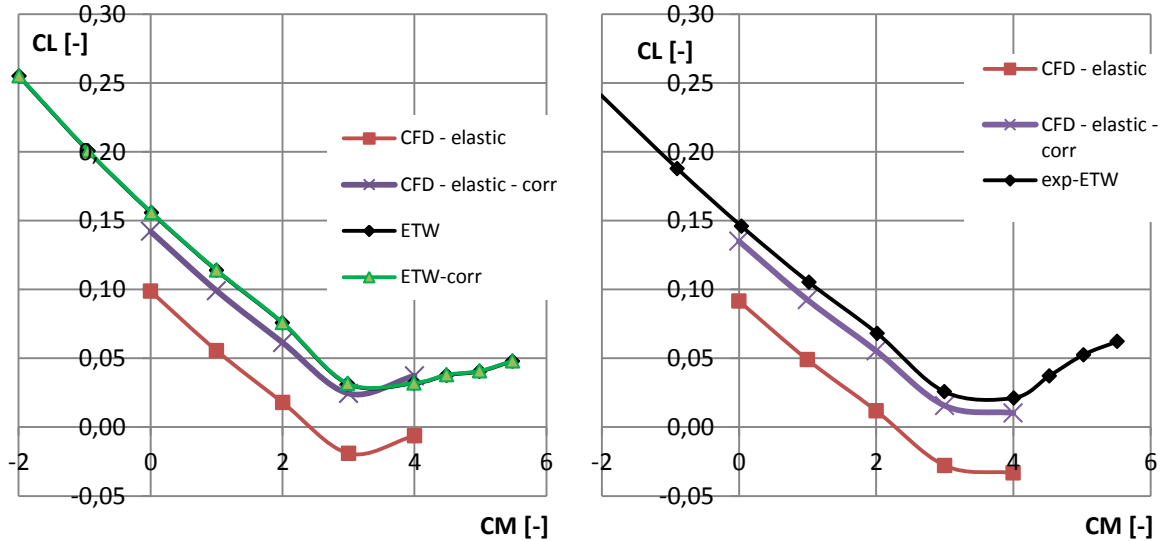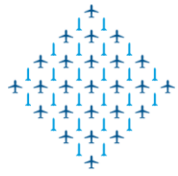
In contrast to using the perturbation grid approach [18], the on-line mesh deformation technique gives more consistent results in comparison with experimental data.
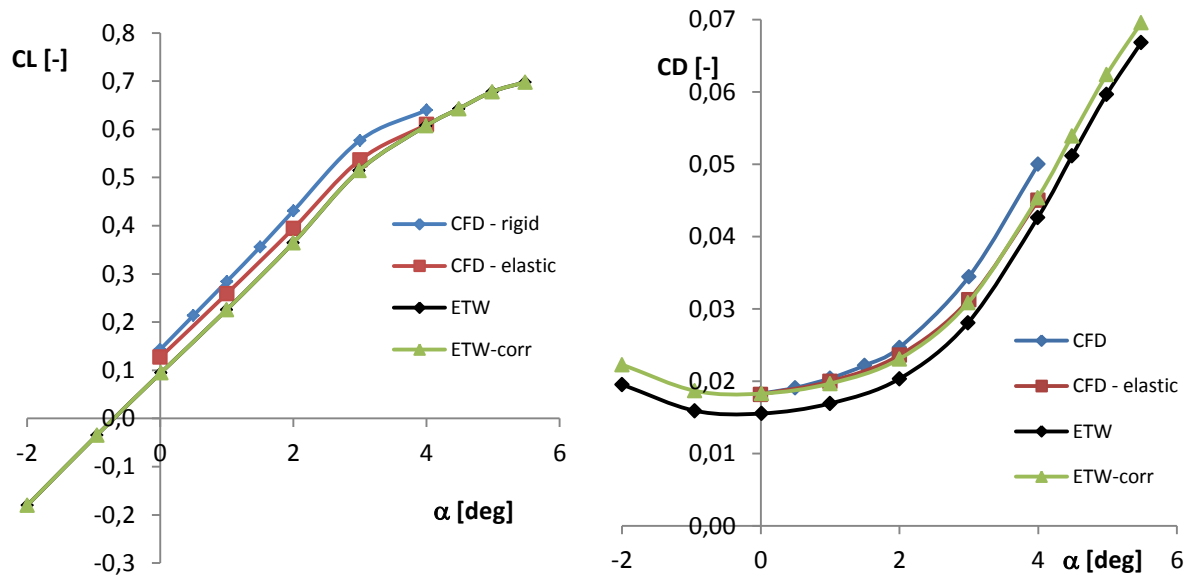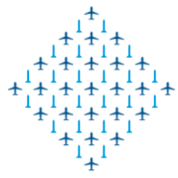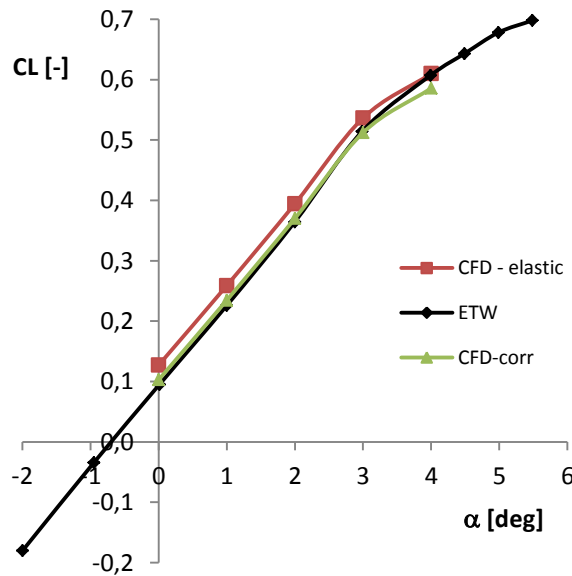
Figure 3: Comparison of CFD results with experimental data, Re=5·10⁶
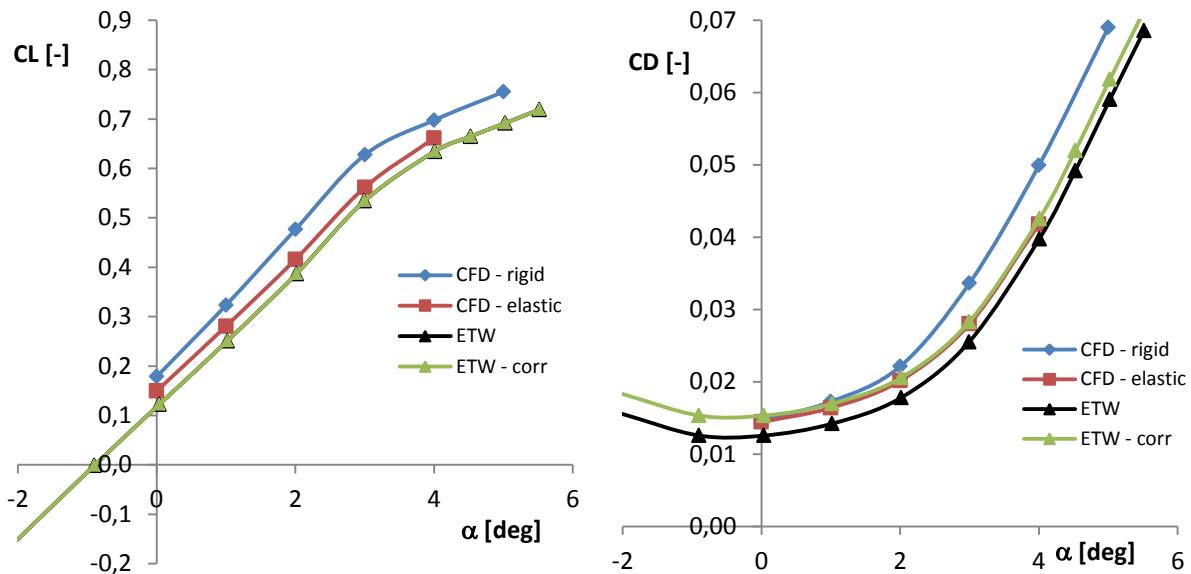
Figure 4: Comparison of CFD results with experimental data, Re=30·10⁶

Figure 5 Comparison of Cm values for Re=5·10⁶ (left) and Re=30·10⁶ (right)

**Figure 6 Effect of correction on support system from [6] and [20] on CL, Re=5·10⁶**

5.2 Wing deformation

The wing deformation of the model during the wind tunnel tests was measured by contactless Stereo Pattern Tracking (SPT) optical method at defined position along a wing span [21]. The wing twist angle and wing bend were measured and both values were used for deeper verification and evaluation of the CFD simulation utilizing the elastic model. The resolution of SPT system is better than 0.1mm for wing

bend and 0.1° for wing twist. The accuracy determination of the wing twist close to the wing tip is approximately 0.3° due to the smaller distances between markers in chord wise direction.

Since the matching values of CL were not obtained during wind tunnel tests and CFD simulations for particular α's, the wind tunnel model deformation data was interpolated to the same values of CL to ensure that the load distribution of the wing is the same.

The deformation of the wing of the CFD model was evaluated at the same 9 cross sections along a wing span which are also used for comparison of CP distributions. The final wing deformation for particular α's was compared with the wing twist angle and wing bend distributions of the rigid model, which represents the jig shape of the wing. The comparison of the twist angle distributions for Re=$5 \cdot 10^6$, $30 \cdot 10^6$ and selected α are depicted in Figure 7 and Figure 8, respectively. The α=0°, 3° and 4° were selected intentionally to see the dependence of the wing deformation on the loads. Almost constant differences in wing twist angle is observed for both regimes for α=0°. These differences are within the accuracy of measurement technique. Slightly bigger differences were observed for higher α, nevertheless the calculated wing twist distributions along the span is very close to the wing twist measured during the experiments.
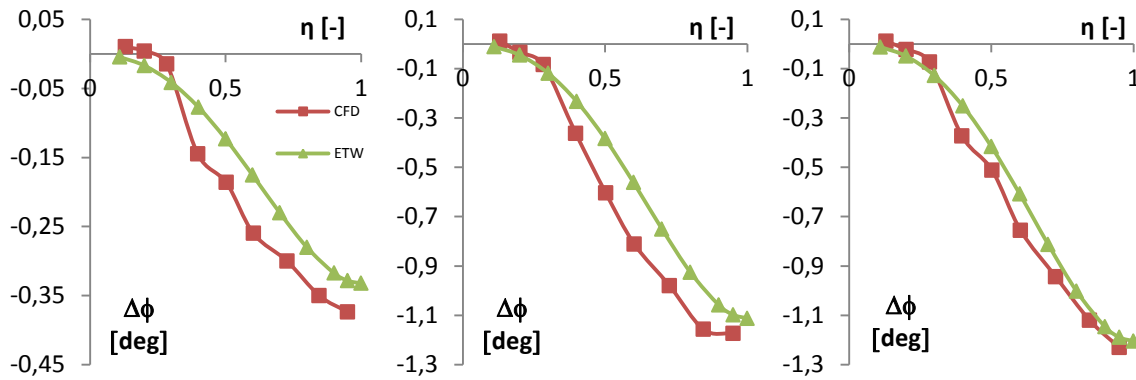
Figure 7 Wing twist distribution for α=0° (left), α=3° (middle) and α=4° (right), Re=$5 \cdot 10^6$
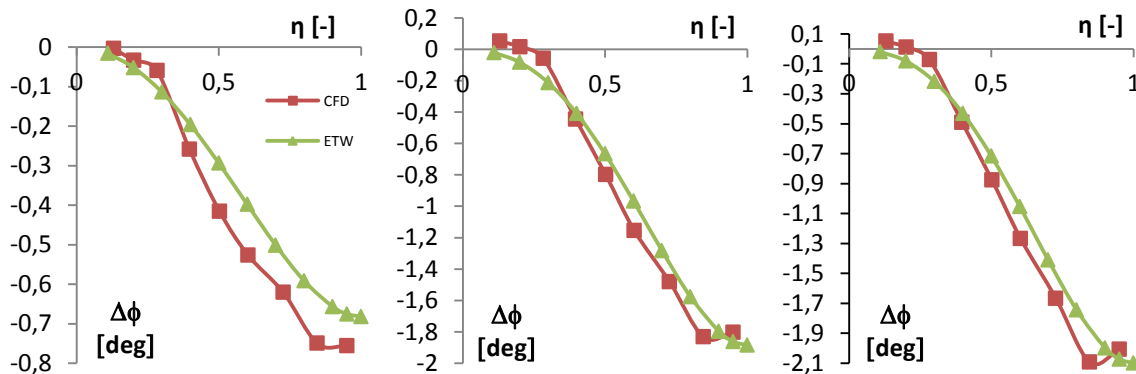
**Figure 8 Wing twist distribution for α=0° (left), α=3° (middle) and α=4° (right), Re=$30 \cdot 10^6$**

The wing bends relative to the rigid model of particular regimes are depicted in Figure 9 and Figure 10. The wing bend is overpredicted for both Reynolds numbers and α=0°. Contrary to the calculated wing bend corresponding to the Re=$30 \cdot 10^6$, the wing bend is slightly over predicted for higher Reynolds

number. With reference to the relatively simple methods used for implementation of the wing deformation into CFD simulation, very good correlation between the measured and simulated wing bend have been observed for Re=30·10^6 and α=3° and 4°.

The wing bend does not have primary effect on the aerodynamic forces, but the twist angle of the wing is affected by bending due to the wing sweep. It is important to accurately predict wing bend as well as the wing twist to obtain better prediction of the local flowfield and aerodynamic forces.
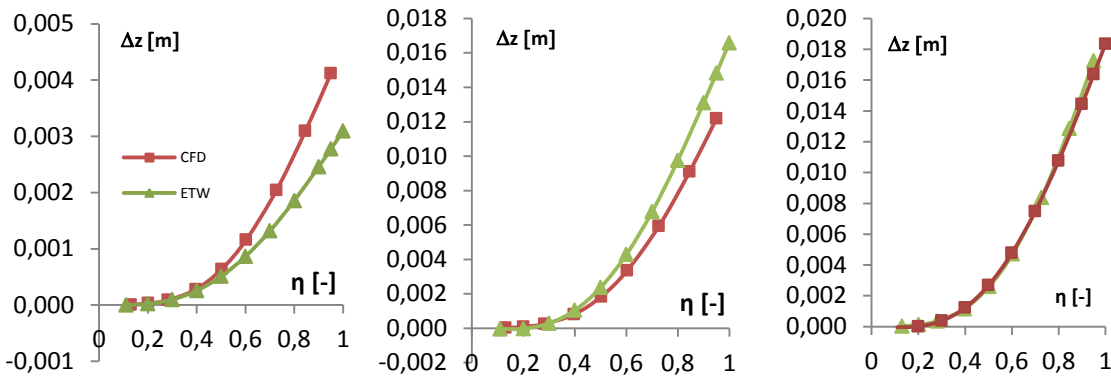
Figure 9 Wing bend for α=0° (left), α=3° (middle) and α=4° (right), Re=5·10^6
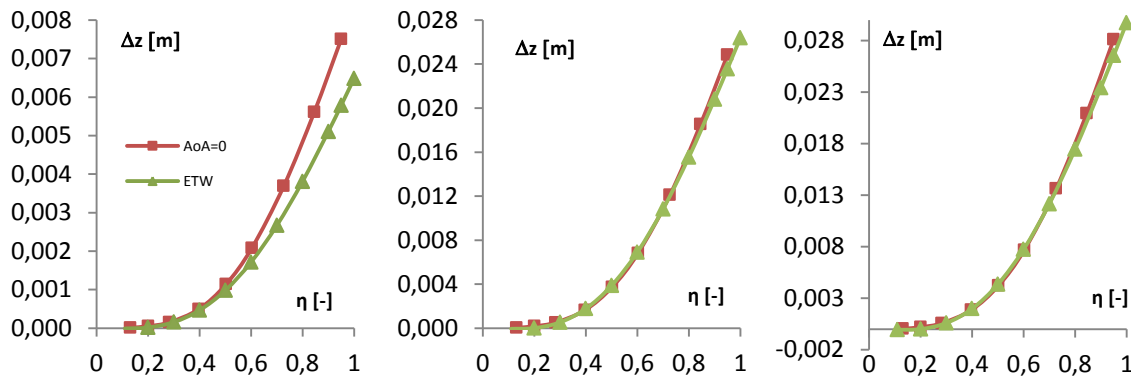
Figure 10 Wing bend for α=0° (left), α=3° (middle) and α=4° (right), Re=30·10^6

5.3   Pressure distribution

The effects of wing deformation can be easily seen in the comparison of Cp's from experiment, rigid and elastic model simulations at specified cross section along the wing span. The CRM is equipped with the pressure taps at 9 cross sections along a wing span. The Cp distribution from the pressure taps located at the inboard part of the wing are not depicted in the following figures because of very small wing's deformation and, hence, negligible differences in Cp have been observed at this part of the wing. The pressure distributions at the outboard part of the wing were used to evaluate CFD simulations and also to explain the effect of the wing deformation on local flowfield.

The comparisons of the Cp distributions of the rigid and elastic model and from the experiment are depicted in Figure 11 and Figure 12. These values correspond to the α=0° and α=4° for Re=30·10^6. It is possible to see a very good agreement between the experimental and CFD values of Cp at the middle part of the wing. Both rigid and elastic models predict the "rooftop" pressure levels very well with almost

no difference. On the other hand the calculated shock wave position is slightly downstream compared to the experiment which contributes to the overprediction of CL and wing twist angle.

Moving towards the wing tip the effects of the aeroelastic deformation are more evident. Bigger deformation of the wing is associated with the outer portion of the wing and it causes bigger differences in Cp distributions of the rigid and elastic model. As it is shown in Figure 8 the outer portion of the wing of the elastic model is more twisted than the CRM. This deformation reduces the negative pressure peaks predicted by the rigid model and reproduces the "rooftop" pressure levels of the experimental data with a very good match for α=4°. On the other hand the higher wing twist angle at the wing tip region causes the higher suction peaks for α=0°.

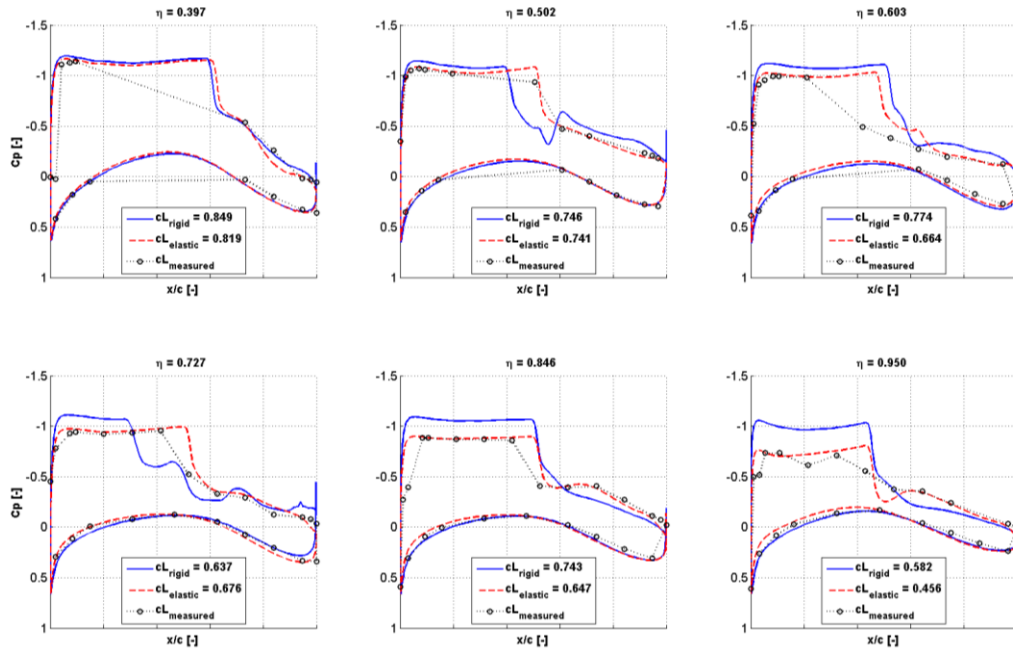Variation of Cp values corresponding to the rigid model at the outboard wing is caused by the shock induced separation predicted at α=4°. Similar behaviour was observed during the 5th DPW [19]. It is supposed that the flow is not steady for this condition and the URANS methods are more adequate than RANS methods. The elastic model was simulated by URANS approach and the unsteady behaviour of the flow was captured and it resulted in smoother Cp distribution. No flow separation causing the unsteadiness in the flowfield was observed for smaller α.

The slope of the shock wave from the experiment in the middle part of the wing for α=4° and Re=30·10[6] is typical for moving shock wave due to, e.g., buffeting. Unfortunately it is not possible to determine if the buffet onset at α=4° due to missing RMS values. The position of the shock wave was stable for whole range of calculated α's. The buffet onset could be postponed to the slightly higher α, unfortunately not simulated within this study. Another reason for stable solution is rather big time step used for unsteady simulation which was sufficient from the elasticity point of view, but it does not fully correspond to the time step from the flowfield point of view.

Despite of this higher twist of the outer wing of CFD simulations the correlation of Cp's between experiment and elastic model is very good and consistent with final wing deformation of the particular regimes and model settings.
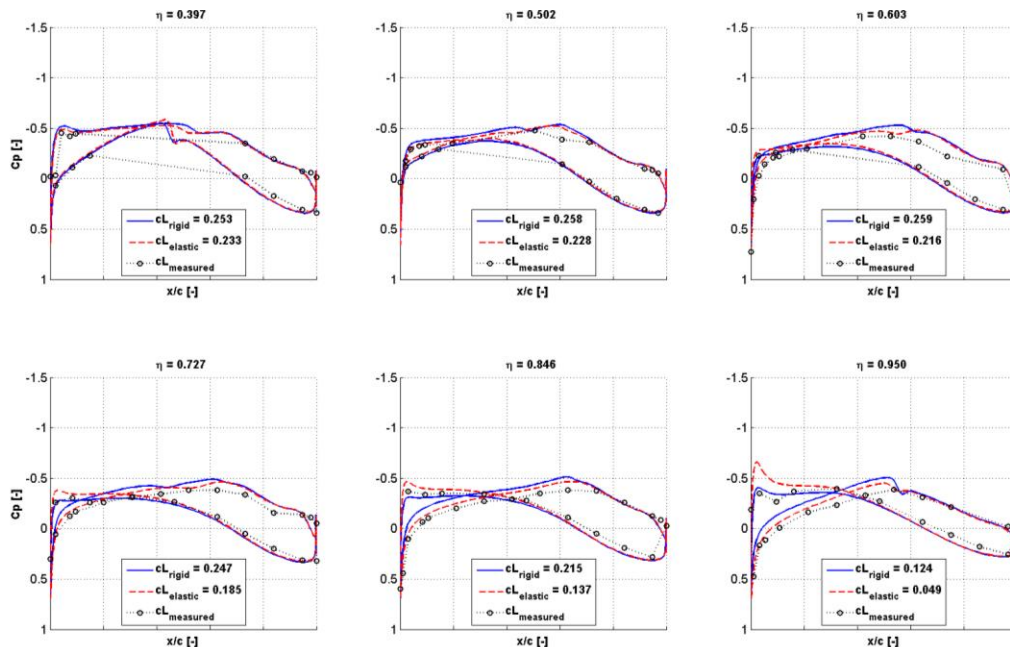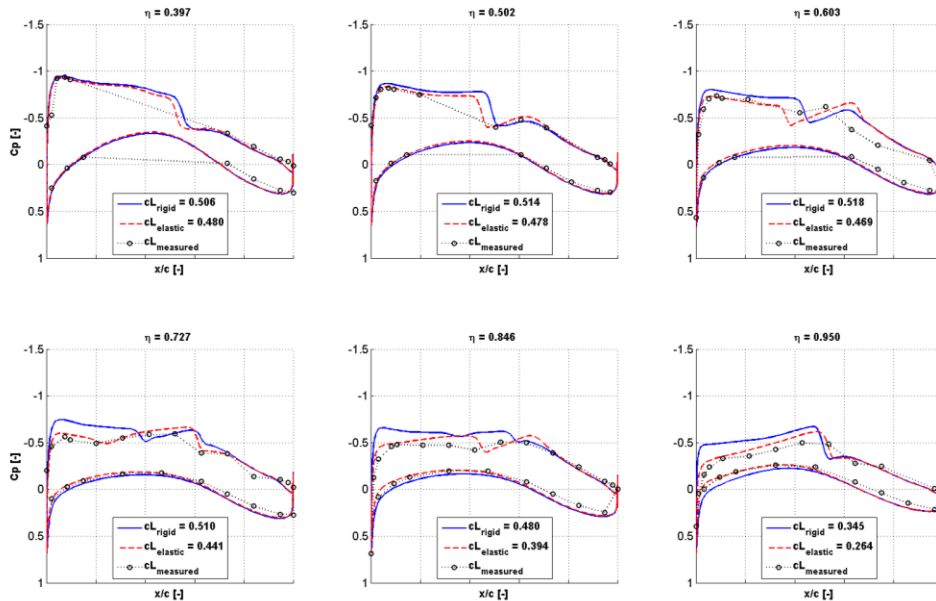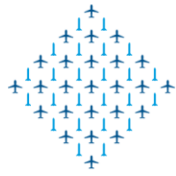

Figure 11: Cp comparison of the rigid and elastic model with experimental data at outer part of the wing for α=0° and Re=30·10[6]

Figure 12: Cp comparison of the rigid and elastic model with experimental data at outer part of the wing for $\alpha=4°$ and Re=30·10^6
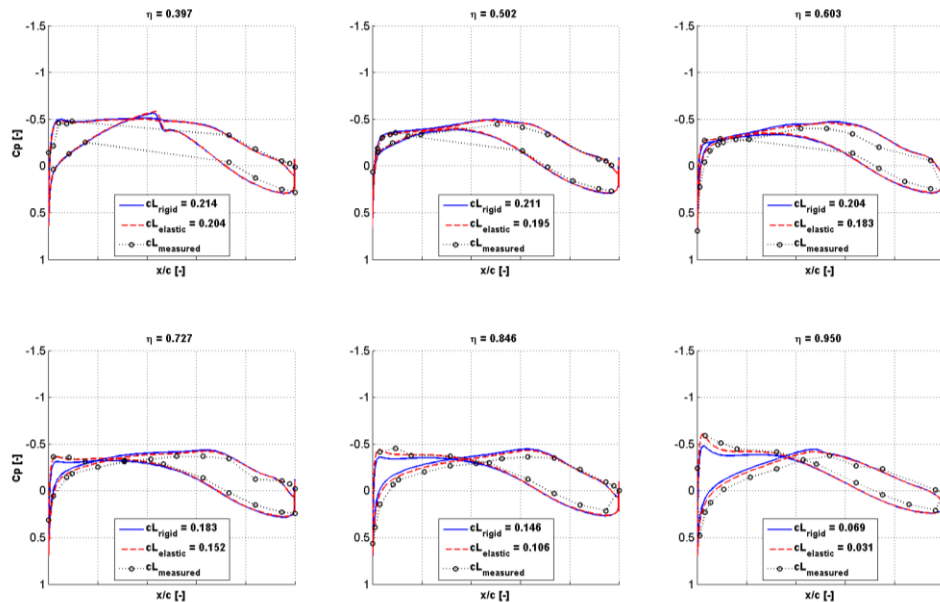
Figure 13 Cp comparison of the rigid and elastic model with experimental data at outer part of the wing for $\alpha=0°$ and Re=5·10^6

Figure 14 Cp comparison of the rigid and elastic model with experimental data at outer part of the wing for $\alpha=2°$ and Re=5·10^6

6   CONCLUSION

The main aim of this study was utilization of the modal analysis of the wing for better prediction of the aerodynamic forces. The first 20 modes of the wing in connection with the on-line mesh deformation have been used during CFD simulations. The wing deformation (wing twist angle) is very well predicted and a very good agreement of the results in terms of aerodynamic forces and Cp distributions has been achieved. The Cp distributions in defined cross sections along the wing span of the elastic model are closer to the experimental values than the Cp distributions of the rigid model. Both, the negative pressure peaks and the "rooftop" pressure levels are predicted very well by elastic model. In spite of consideration of the wing deformation some differences in CL, Cm and the wing twist angle of the outer portion of the wing persist. The reasons for these differences could be caused by the missing support system during CFD simulations. In case that the correction on support system developed in [6] and [20] is used on values of CL and Cm, almost perfect match in CL is achieved and the values of Cm are very close to the experimental values. Very good agreement has been achieved between CFD and experimental drag values.

The differences in the Cp distributions in the vicinity of shock wave for higher α's need to be evaluated and explained. The exact shock wave position is sensitive to the turbulence modelling, grid resolutions, etc.

This method can be used in case that the high fidelity methods like FSI cannot be used. It has been showed that quite small number of modes is sufficient for increasing the accuracy of the CFD results.

The problem was studied mainly from a methodological point of view. A follow on investigation will look at more detail analysis of these results and utilization of the same procedure for simulations of the deformation of the whole model to include the effect of asymmetric modes and the effect of deformation of others parts of the model, mainly deformation of HTP. The effect of the wake from the wing on the

empennage for low and high-speed conditions will be investigated as the main output of the ESWI[RP] project.

7   ACKNOWLEDGEMENT

8   REFERENCES

[1]   ESWIRP project website: www.eswirp.eu.

[2]   Lutz, T., "Time-resolved Prediction and Measurement of the Wake past the CRM at high Reynolds number stall conditions", AIAA Paper 2015-1094, 2015.

[3]   Konrath, R., "High-Speed PIV Applied to Wake of NASA CRM Model in ETW Under High Re-Number Stall Conditions for Sub- and Transonic Speeds", AIAA Paper 2015-1095, 2015.

[4]   Green, J., Quest, J., "A short history of the European Transonic Wind Tunnel ETW", Progress in Aerospace Sciences, Volume 47, Issue 5, pp. 319-368, July 2011

[5]   Rivers, M. B. and Dittberner, A., "Experimental Investigations of the NASA Common Research Model in the NASA Langley National Transonic Facility and the NASA Ames 11-ft Transonic Wind Tunnel (Invited)", AIAA Paper 2011-1126, 2011.

[6]   Rivers, M. B., Hunter, C. A., and Campbell, R. L., "Further Investigation of the Support System Effects and Wing Twist on the NASA Common Research Model", AIAA Paper 2012-3209, 2012.

[7]   Eberhardt, S., Benedict, K., Hedges, L., and Robinson, A., "Inclusion of Aeroelastic Twist into the CFD Analysis of the Twin-Engine NASA Common Research Model", AIAA Paper 2014-0251, 2014.

[8]   Keye, S. and Rudnik, R., "Validation of Wing Deformation Simulations for the NASA CRM Model using Fluid-Structure Interaction Computations", AIAA Paper 2015-0619, 2015.

[9]   Vassberg, J. C., DeHaan, M. A., Rivers, M. B., and Wahls, M. S., "Development of a Common Research Model for Applied CFD Validation Studies", AIAA Paper 2008-6919, 2008.

[10]   NASA Common Research Model website: http://commonresearchmodel.larc.nasa.gov.

[11]   Drag Prediction Workshop website: http://aaac.larc.nasa.gov/tsab/cfdlarc/aiaa-dpw/Workshop5/grids.html.

[12]   Tyssel, L., "Hybrid Grid Generation for Complex 3D Geometries", Proceedings of the 7th International Conference on Numeric Grid Generation in Computational Field Simulation, Whistler, British Columbia, Canada, 2000, pp. 184-196.

[13]   Tyssel, L., "Experiences of Grid Generation and Steady/Unsteady Viscous Computations for Complex Geometries", Proceedings of the 26th ICAS Congress, Anchorage, Alaska, USA, 2008.

[14]   Eliasson, P., "EDGE, a Navier-Stokes Solver for Unstructured Grids", Proceedings to Finite Volume for Complex Applications III., ISTE Ltd., London, 2002, pp. 527-534.

[15]   Wallin, S. and Johansson, A. V., "An Explicit Algebraic Reynolds Stress Model of Incompressible and Compressible Flows", Journal of Fluid Mechanics, Vol. 43, No. 9, 2000, pp. 89-132.

[16]   Balakrishna, S. and Acheson, M., "Analysis of NASA Common Research Model Dynamic Data", AIAA Paper 2011-112, 2011.

[17]   Smith, J., "Aeroelastic fucntionality in Edge, Initial implementation and validation", FOI-R-1485-SE, Dec. 2005.

[18] Vrchota, P. and Prachař, A., "Improvement of CFD aerodynamic characteristics using modal deformation", Proceedings of the 55th Israel Annual Conference on Aerospace Sciences, Tel Aviv & Haifa, Israel, 2015.

[19] Levy, D., Laflin, K., Vassberg, J., Tinoco, E., Mani, M., Rider, B., Brodersen, O., Crippa, S., Rumsey, C., Wahls, R., Morrison, J., Mavriplis, D., and Murayama, M., "Summary of Data from the Fifth AIAA CFD Drag Prediction Workshop", AIAA Paper 2013-0046, 2013.

[20] Kohzai, M., Ueno, M., Koga, S., Sudani, N., "Wall and Support Interference Corrections of NASA Common Research Model Wind Tunnel Test in JAXA", AIAA Paper 2013-0963, 2013

[21] Quix, H. and Semmelmann, J., "Model Deformation Measurement Capabilities at ETW", AIAA Paper 2015-2562, 2015